



Geophysical Research Letters

RESEARCH LETTER

10.1029/2018GL078059

Special Section:

Cassini's Final Year: Science Highlights and Discoveries

Key Points:

- Cassini detected few micron-sized particles near the ring plane between Saturn and the D ring
- RPWS measured the dust density profile and size distribution at the edge of the D ring
- Waveforms of the dust impact signals change with the background plasma density

Supporting Information:

- Supporting Information S1

Correspondence to:

S.-Y. Ye,
shengyi-ye@uiowa.edu

Citation:

Ye, S.-Y., Kurth, W. S., Hospodarsky, G. B., Persoon, A. M., Sulaiman, A. H., Gurnett, D. A., et al. (2018). Dust observations by the Radio and Plasma Wave Science instrument during Cassini's Grand Finale. *Geophysical Research Letters*, 45, 10,101–10,109. <https://doi.org/10.1029/2018GL078059>













Received 23 MAR 2018

Accepted 21 AUG 2018

Accepted article online 14 SEP 2018

Published online 4 OCT 2018

Dust Observations by the Radio and Plasma Wave Science Instrument During Cassini's Grand Finale

S.-Y. Ye¹ , W. S. Kurth¹ , G. B. Hospodarsky¹ , A. M. Persoon¹ , A. H. Sulaiman¹ , D. A. Gurnett¹ , M. Morooka² , J.-E. Wahlund² , H.-W. Hsu³ , Z. Sternovsky³ , X. Wang³ , M. Horanyi³, M. Seiß⁴, and R. Srama⁵ 

¹Department of Physics and Astronomy, The University of Iowa, Iowa City, IA, USA, ²Swedish Institute of Space Physics, Uppsala, Sweden, ³LASP, University of Colorado Boulder, Boulder, CO, USA, ⁴Institute of Physics and Astronomy, University of Potsdam, Potsdam, Germany, ⁵Institute Space Systems (IRS), University of Stuttgart, Stuttgart, Germany

Abstract Dust particles in the Saturn system can be detected by the Radio and Plasma Wave Science (RPWS) instrument on board Cassini via antenna voltage signals induced by dust impacts. These impact signals have been simulated in the laboratory by accelerating dust particles onto a Cassini model with electric field antennas. RPWS dust measurements have been shown to be consistent with the Cosmic Dust Analyzer. During the Grand Finale orbits, Cassini flew through the gap between the D ring and Saturn's atmosphere 22 times. In situ measurements by RPWS helped quantify the hazards posed to the spacecraft and instruments on board, which showed a micron-sized dust density orders of magnitude lower than that observed during the Ring Grazing orbits. Close inspection of the waveforms indicated a possible dependence of the impact signal decay time on ambient plasma density.

Plain Language Summary Cassini flew through the gap between Saturn and its rings for 22 times before plunging into the atmosphere of Saturn, ending its 20-year mission. The radio and plasma waves instrument on board Cassini helped quantify the dust hazard in this previously unexplored region. The measured density of large dust particles was much lower than expected, allowing high-value science observations during the subsequent Grand Finale orbits.

1. Introduction

Although the dense main rings of Saturn are composed of meter-sized ice chunks, the rest of Saturn's ring plane is filled with fainter and more tenuous rings containing much smaller particles (less than 100 μm across, similar to particles in smoke; Cuzzi et al., 2009; Horányi et al., 2009). In addition to gravity, these tiny particles are subject to solar radiation pressure and electromagnetic forces, making their dynamics substantially different from those of the main ring particles (Horányi, 1996). Relatively rapid orbit evolution and plasma sputtering make the lifetime of these particles less than a few thousand years (Burns et al., 2001). These diffuse rings are then replenished continuously, for example, by geological activity or meteoroid bombardment of embedded moons and larger ring particles (Spahn, Albers, et al., 2006; Spahn, Schmidt, et al., 2006; Hedman et al., 2007; Williams & Murray, 2011).

The small size of the particles in the diffuse rings allows them to be observed both remotely (visual and infrared imaging) and in situ (plasma, dust, and wave instruments). Remote sensing from the ground and spacecraft can put constraints on the density and size distribution of the particles in the diffuse rings through model fitting (de Pater et al., 2004; Hedman et al., 2012; Nicholson et al., 1996; Showalter et al., 1991; Showalter, 1996). While Cassini has a dedicated dust instrument on board, the Cosmic Dust Analyzer (CDA; Srama et al., 2004), that is designed to measure the size, density, velocity, charge, and composition of the dust particles, other instruments (e.g., Radio and Plasma Wave Science [RPWS], Cassini Plasma Spectrometer [CAPS], Electron Spectrometer [ELS], Ion and Neutral Mass Spectrometer [INMS], Magnetospheric Imaging Instrument [MIMI], Low Energy Magnetospheric Measurement System [LEMMS]) have demonstrated the ability to register dust impacts when the spacecraft flew through dusty regions (Dong et al., 2015; Hill et al., 2012; Jones et al., 2009; Krupp et al., 2017; Kurth et al., 2006; Wang et al., 2006; Ye et al., 2014; Ye, Gurnett, & Kurth, 2016).

On 26 April 2017, Cassini dove into the gap between Saturn's main ring and its atmosphere, starting the Grand Finale orbits. This region had never been visited by any spacecraft before, so the dust hazard posed a concern for the safety of the spacecraft and the instruments on board. During the first ring plane

crossing, the High Gain Antenna (HGA) was pointed toward the ram direction, shielding the spacecraft and most of the payloads from possible damage by dust impacts. The RPWS was the only instrument on board that was able to measure the dust density and size distribution during this ring plane crossing, because CDA was shielded by the HGA and the angle between the dust ram and the CDA boresight is larger than 60° .

In this paper, we analyze RPWS data collected between the D ring and the atmosphere of Saturn. We start with a brief discussion of the detection mechanisms. We then show the RPWS measurements around the ring plane crossings and compare them with the Ring Grazing orbits observations. Finally, we inspect the waveforms of the impact signals in detail and discuss the possible connection between the shape of the impact signal and background plasma properties. We expect these in situ observations to provide new insights into dust in a previously unexplored region close to Saturn.

2. Dust Detection by Electric Antennas

The technique of using electric field antennas to detect dust impacts dates back to the Voyager 2 encounter of Saturn (Aubier et al., 1983; Gurnett et al., 1983). The kinetic energy of an impact is converted to thermal energy which vaporizes the dust particle and part of the surface material, creating a partially ionized gas of ions and electrons. Depending on the potential of the spacecraft body and antenna elements, these charged particles are either collected or expelled from the impact site, setting up a potential difference between different elements of the dipole and monopole antennas. The spacecraft body is also considered as an antenna element (of the monopole antenna). Ye, Kurth, Hospodarsky, Averkamp, and Gurnett (2016) showed that the monopole antenna is sensitive primarily to dust impacts on the spacecraft body and the dipole antenna is sensitive primarily to dust impacts on the antenna booms. The rise time of the signal is a function of the ion/electron thermal speed, which is determined by the kinetic to thermal energy conversion during the impact (Meyer-Vernet et al., 2017). Laboratory simulations of the antenna signals induced by dust impacts indicate that the rise time is dependent on the polarity of the target potential (this determines whether ions or electrons escape, which have different thermal velocities; Ye, Kurth, Hospodarsky, Averkamp, Gurnett, Sternovsky, et al., 2016). The elements of the electric antennas (including the antenna booms and the spacecraft body) will recover to their equilibrium potential by recollecting charges from the background plasma (Zaslavsky, 2015). The recharging timescale is determined by the ambient plasma density, the surface area, and capacitance of the antenna elements, which are significantly different for the spacecraft body and antenna booms. The overshoots often observed in the waveforms of the dust impacts can be explained by this difference in recharging timescales. However, O'Shea et al. (2017) recently demonstrated through kinetic simulation that the antenna elements are inefficient charge collectors and some unknown mechanism besides the difference in the recharging timescales could be responsible for the characteristic overshoots in the dust impact signals observed by Solar Terrestrial Relations Observatory, another spacecraft that is sensitive to dust impacts.

3. Observations

Before the Grand Finale orbits, the region between Saturn and the D ring was only observed by remote sensing instruments (e.g., Imaging Science Subsystem). The phase curves of diffuse rings like Saturn's G ring and D ring have been shown to be forward scattering (Hedman & Stark, 2015). Images obtained at high phase angles (low scattering angles) show that the brightness of the inner edge of the D ring decreases exponentially from the radial distance 67,000 km with a scale length around 1,000 km (Hedman et al., 2013; Hedman & Showalter, 2016). For comparison, the radius of Saturn at its equator is 60,268 km. The brightness at 65,000 km radial distance was estimated to be equal to the brightness of the G ring core, so the estimated brightness at 63,300 km radial distance, where the first dive took place, was thought to be a few times that of the Janus/Epimetheus ring (M. M. Hedman, personal communication, March 2017). Assuming the dust density is proportional to the brightness of the ring, the dust density at this radial distance should also be a few times higher than that observed in the Janus/Epimetheus ring. An individual impact signal is proportional to the impact charge released, which is proportional to the product of the particle mass and the ram speed to the approximate fourth power (Collette et al., 2014). Given the 1.5 times higher ram speed during the Grand Finale orbits, each impact signal would be ~ 5 times larger. The spectral power of the ensemble dust impact signature is proportional to the product of impact signal squared and impact rate (Meyer-Vernet et al., 2009), which is proportional to the dust density times the ram speed. So for the Grand Finale

orbits, the spectral power of dust impacts was estimated to be 40–80 times higher than that of the Ring Grazing orbits. However, surprisingly, when Cassini took the first dive between the D ring and Saturn (orbit 271) on 26 April 2017, no intense broadband signal typical of dust impacts (e.g., spikes indicated by arrows in Figure 1) was observed near the ring plane. Close inspection of the waveforms revealed only a few dust impacts, not enough for characterizing the density profile or the size distribution function. The following four orbits (orbits 272–275) yielded similar results, with different spacecraft attitudes, receiver bandwidths, and antenna modes. During orbits when CDA was pointed toward the ram direction near the ring plane, the High Rate Detector only detected a few large ($\sim 1 \mu\text{m}$) particles (Hsu et al., 2018).

Figure 1 shows two RPWS electric field power spectrograms for the orbit 280 ring plane crossing, which provided clearer dust impact signals for characterizing the particle properties in this region ($\sim 63,810$ km radial distance). The top panel shows the low rate data, and the bottom panel shows the high rate Wideband Receiver (WBR) data. The low rate data covers a wide frequency range (2 Hz to 16 MHz). Since Cassini was very close to Saturn during this orbit, the magnetic field is very strong. As a result, the electron cyclotron frequency (indicated by the white curve in the top panel) is higher than the local electron plasma frequency, which is determined from the upper cutoff of the whistler mode wave (Persoon et al., 2018). The plasma density derived from the cutoff frequency agrees well with the Langmuir probe measured electron density. With the enhanced electron/ion density and low electron/ion temperatures measured by the Langmuir probe, it was concluded that Cassini was in the ionosphere of Saturn during these periods (Wahlund et al., 2018). The ionosphere of Saturn was found to be quite dynamic, as the peak plasma densities measured during perikrines of similar altitudes exhibited variations of up to 2 orders of magnitude. The spike around 10:54 is from dust impacts, which is independent of the electron plasma and cyclotron frequencies and therefore cannot be due to any plasma waves. The broadband spectral shape is a result of Fourier transforming the voltage impulses. Such voltage power spectra have been modeled and used for dust density estimations when high rate data are not available (Meyer-Vernet et al., 1996, 2009; Schippers et al., 2014, 2015).

The high rate data (Figure 1 bottom) gives us a high-resolution picture of the waves detected around the ring plane crossing. Besides the main dust signal at the ring plane (10:54), there are many broadband impulsive signals detected away from the ring plane, which are also due to dust impacts. The narrowband harmonic emissions drifting in frequency have been identified as lower hybrid resonances, which for a strongly magnetized plasma are very close to the ion plasma frequency (Sulaiman et al., 2017). These narrowband drifting harmonics should provide important clues to constraining the ion density and even ion species in Saturn's ionosphere.

Figure 2 shows the statistics of dust impacts observed during the ring plane crossing on day of year (DOY) 174, 2017. Figure 2a shows the impact counts as a function of voltage and time. Figure 2b shows the gain of the receiver, which is automatically set based on waveform amplitudes to maximize the use of the analog-to-digital converter dynamic range while minimizing clipping (signal exceeding the range of the analog-to-digital converter; Gurnett et al., 2004). These two panels show that the sensitive size range of the instrument is inversely correlated with the gain (impact signals due to small particle impacts cannot be resolved in lower gains, and those due to large particle impacts are clipped in higher gains), which reached its lowest level at the ring plane crossing.

Figure 2c shows the dust density ($1\text{-}\mu\text{m}$ -size threshold) calculated from the impact rates, assuming an effective impact area of 1 m^2 (The dipole antenna is sensitive to dust impacts on the antenna booms and maybe the part of spacecraft body near the antennas). The sizes are calculated from the magnitude of voltage spikes based on the charge yield relations measured for the surface materials of the spacecraft, Kapton, BeCu, and HGA paint (Collette et al., 2014; Grün et al., 1984). We took into account of the different ram speed (spacecraft velocity – Keplerian velocity) when calculating the particle sizes from the voltage signal sizes. Details of the voltage to size conversion can be found in Ye, Gurnett, and Kurth (2016). Since the sensitive size range of RPWS changes with gain (smaller particles not detectable in the low gains), we scaled the impact rates to a fixed size threshold of $1 \mu\text{m}$, assuming the size distribution has the same slope within and outside the sensitive size range. The red and orange lines are dust densities ($1\text{-}\mu\text{m}$ threshold) inferred from Langmuir probe measurements (difference in ion and electron densities), assuming a power law differential size distribution with an index of -5.5 and -6.0 , respectively. The comparison between the density profiles indicates that the

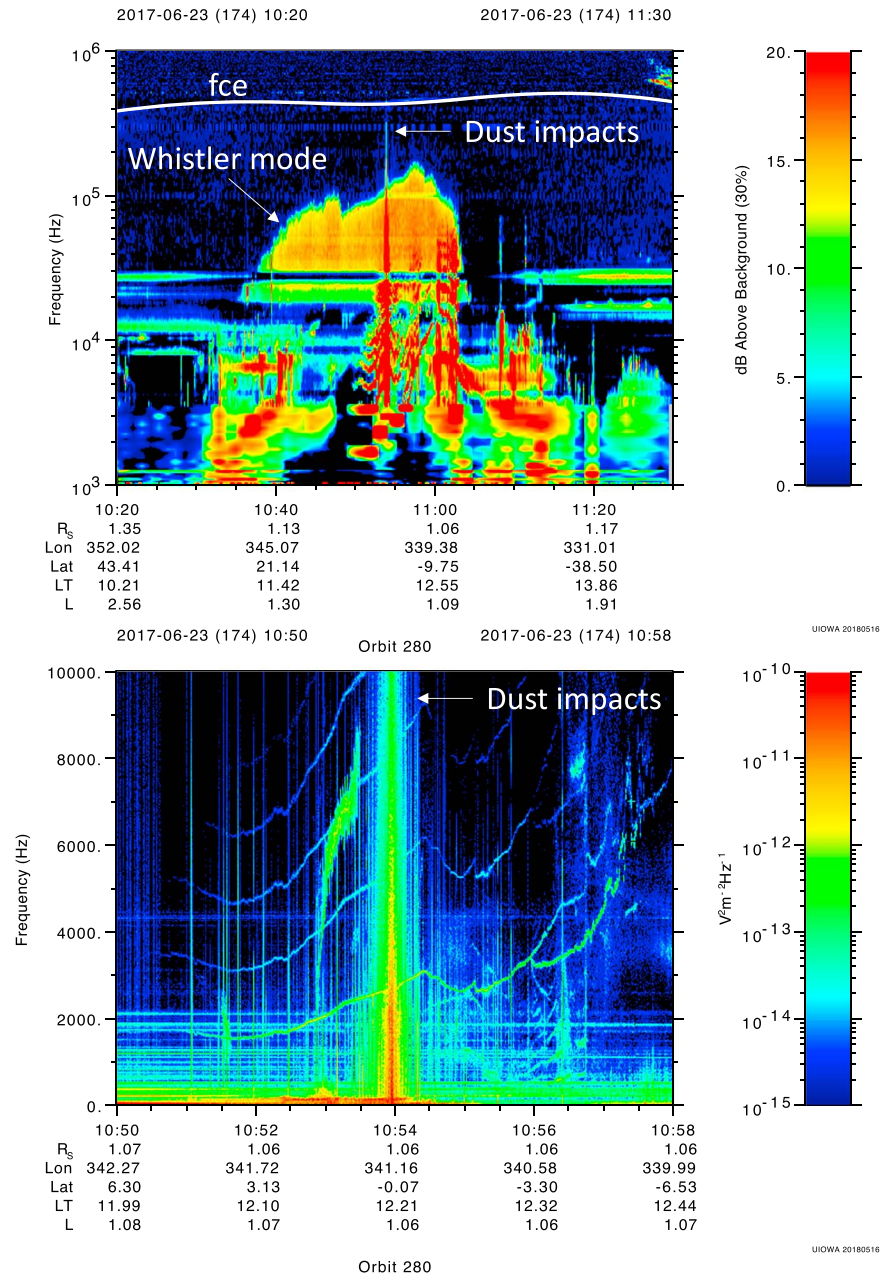


Figure 1. Cassini Radio and Plasma Wave Science electric field power spectrograms for the orbit 280 ring plane crossing (day of year 174, 2017). (top) Low rate data. The low-frequency broadband continuum is whistler mode, the upper cutoff of which is the local plasma frequency. The electron cyclotron frequency is indicated by the white curve. The broadband burst that extends above the electron cyclotron frequency at 10:54 is due to dust impact signals. (bottom) High rate wideband receiver data. The broadband bursts are dust impact signals. The narrowband drifting harmonics are ionospheric lower hybrid waves. fce = electron cyclotron frequency.

size distribution slope could be steeper away from the ring plane, perhaps because it is easier for the smaller grains to migrate away from the ring plane (Morooka et al., 2018).

Figure 2d shows the power law index of differential size distribution estimated within a 10-s moving window (blue diamonds). The voltage impulse sizes recorded in the moving window are sorted into equal size bins of a histogram. The bin with the most voltage signals is selected as the voltage threshold V_{thd} . Then the number of voltage jumps larger than V_{thd} , $2V_{thd}$, and $4V_{thd}$ are fitted with the associated threshold values. Since we

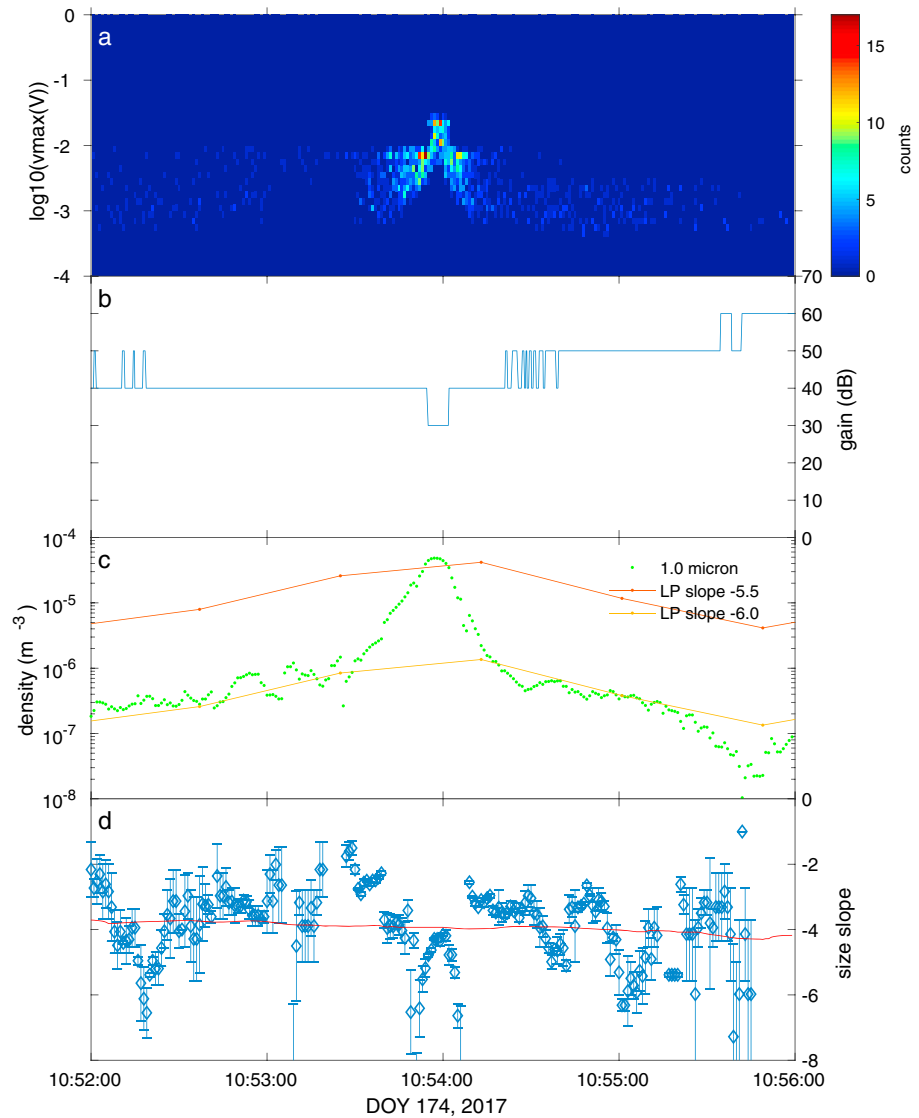


Figure 2. Dust analysis for the ring plane crossing on DOY 174, 2017 (orbit 280). The dipole antenna was used. (a) Impact counts as a function of voltage and time. (b) Gain of the receiver. (c) Dust density (1- μm -size [radius] threshold) calculated from the impact rates. The red and orange lines are estimations of dust densities (1- μm threshold) based on the difference in ion and electron densities measured by the Langmuir probe, assuming a power law differential size distribution with an index of -5.5 and -6.0 , respectively. (d) Power law index of the differential size distribution estimated within a 10-s moving window (blue diamonds; red line shows smoothed value with a 120-s moving window). DOY = day of year.

know that particle mass is proportional to the voltage jump size (Ye, Gurnett, & Kurth, 2016), the fit would give us the power law index of the cumulative mass distribution $\eta + 1$, which can be converted to the power law index of the differential size distribution $\mu = 3\eta + 2$. The red line indicates smoothed values of the individual size slopes (blue diamonds) using a 120-s moving window. This smoothed size slope is also used to scale the density values to the fixed size threshold shown in Figure 2c. Note that these power law size distribution slopes are shallower than those inferred from the fit with Langmuir probe measurements, which showed a depletion of electrons near the ring plane due to the absorption by nanoparticles. There are two possible sources of this discrepancy. One is the uncertainty in the micron-sized dust density measured by the RPWS WBR, which could be as large as 1 order of magnitude. If our estimates of the micron-sized dust density were low, this would cause us to overestimate the slope (i.e., require more nanoparticles) to fit with the Langmuir probe measurements. The other possibility is that the power law size distribution may have a break somewhere, so that the size distribution for nanoparticles is steeper than micron-sized particles.

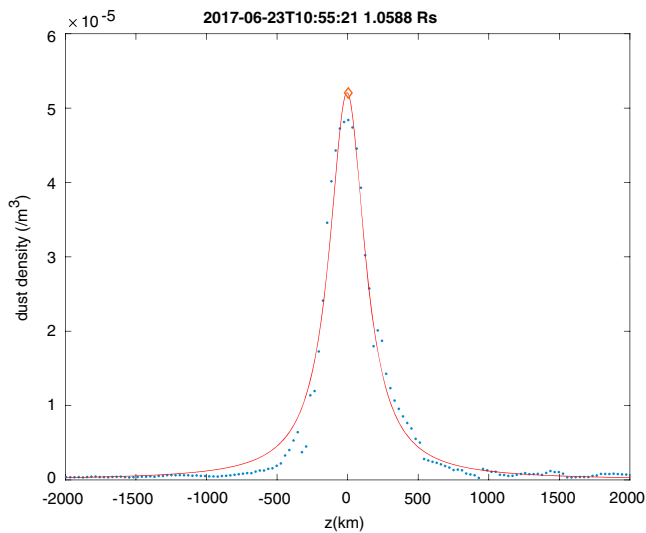


Figure 3. Dust density versus vertical distance from the ring plane, for the ring plane crossing on day of year 174, 2017. The red curve is a Lorentzian function fit of the density profile (full width at half maximum ~ 300 km). The red diamond marks the peak location of the fit (4 km south of the ring plane).

Figure 3 shows a Lorentzian function (red curve) fit of the dust density profile for the ring plane crossing on DOY 174, 2017 (orbit 280). The Lorentzian density model is given by

$$n = \frac{n_0 w^2}{(z - z_0)^2 + w^2} \quad (1)$$

where n_0 is the peak density and z_0 is the vertical offset of the peak density. From this model fitting, the peak density and half width at half maximum (w) of each density profile can be determined. For this ring plane crossing, the measured vertical thickness (w) of the dusty ring is ~ 153 km and the peak density (n_0) is $\sim 5 \times 10^{-5} \text{ m}^{-3}$, about 2–3 times thinner and 2 orders of magnitude lower than those measured by RPWS in the Janus/Epimetheus ring (Ye et al., 2018). During the orbits when CDA had Kepler ram pointing, High Rate Detector measured a few large (micron-sized) particles per orbit. Combining these measurements, a density profile was derived with a full width at half maximum of 900 km and maximum density of $(20 \pm 10) \times 10^{-5} \text{ m}^{-3}$ (Hsu et al., 2018). The wider peak estimated from CDA measurements could be due to the inclusion of multiple orbits. Cassini crossed the ring plane at different distances from the D ring during these orbits, where the density and ring width could also be different. The difference in density measured by the two instruments is within the uncertainty range estimated for RPWS measurements (Ye et al., 2014).

We inspected the dust impact waveforms from ring plane crossings at different altitudes and found that the decay timescale changed from orbit to orbit. Figure S1 shows that during the first Grand Finale orbit, the decay timescale of the dust impact signals changes with the radial distance of detection, with the longest decay time seen at the largest radial distance. Cassini traversed through the ionosphere of Saturn during all of the periapses, and it is shown that the ionospheric density decreases with the altitude and exhibits large variability (Wahlund et al., 2018). As modeled by Zaslavsky (2015), the decay time of the impact signals depends on background plasma density, which determines the recharging current. It is possible that the variation of decay time is mainly due to the variation of the background plasma density, though other factors like the antenna mode (dipole/monopole) and receiver bandwidth could also contribute.

Figure 4 shows a WBR waveform snapshot near the ring plane crossing of orbit 282 (DOY 187, 2017). The receiver was in monopole mode, which measures the voltage between the E_w antenna and the spacecraft (Please refer to Figure 14 of Gurnett et al., 2004 for geometry of RPWS antennas with respect to the Cassini spacecraft). Note that the dust impact signals were mostly positive (red diamonds) rather than negative (green diamond). As discussed by Ye, Kurth, Hospodarsky, Averkamp, and Gurnett (2016), RPWS primarily detect impacts on the antenna elements, which means the E_u and E_v antennas for the dipole mode and the E_w antenna and the spacecraft body for the monopole mode. This was also confirmed by laboratory simulations of dust impacts on a Cassini model equipped with both dipole and monopole antennas (Nouzak, Hsu, et al., 2017; Nouzak, Pavlu, et al., 2017). In the monopole mode, the polarities of the impact signals are determined by the spacecraft potential. It has been shown during the ring plane crossings outside the main rings of Saturn that the polarities of the impact signals detected by the monopole antenna were mostly negative, consistent with a negative spacecraft potential in those regions (Ye et al., 2014 and Ye, Kurth, Hospodarsky, Averkamp, & Gurnett, 2016). So the mostly positive impact signals shown in Figure 4 seem to indicate that the spacecraft was charged positively on the inner edge of the D ring, which is surprising because the spacecraft was in the ionosphere of Saturn, where cold and dense plasma dominates. Langmuir probe also measured positive spacecraft potential in the corridor between the D ring and the atmosphere of Saturn, especially during the lower altitude orbits. It is possible that the positive potential is due to secondary electron emissions induced by kinetic ion/fast neutral impacts when the spacecraft cut through the deep ionosphere, similar to what the Langmuir probe observed in the deep ionosphere (Wahlund et al., 2018).

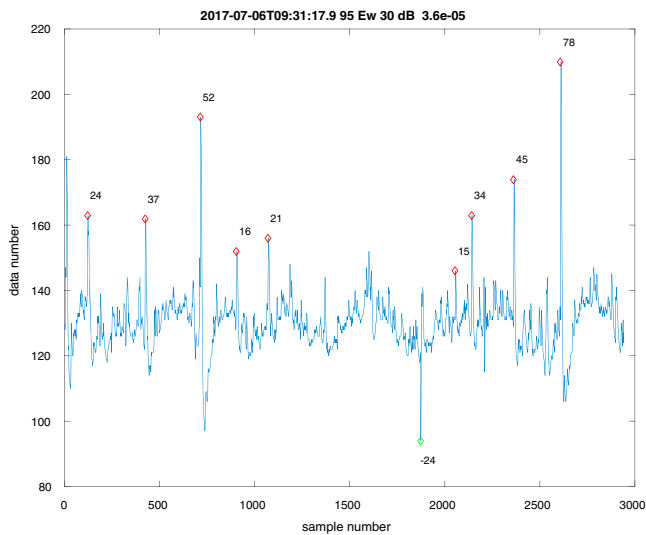


Figure 4. Wideband receiver waveform snapshot near the ring plane crossing of orbit 282 (day of year 187, 2017). The receiver was in monopole mode, which measures the voltage between the E_w antenna and the spacecraft. The dust impact signals were labeled with red diamonds for positive impacts and a green diamond for the negative impact.

4. Discussion

The RPWS dust observations during the Grand Finale orbits revealed a significant lower density of micron-sized dust particles between the D ring and the atmosphere of Saturn than the hazard analysis estimation based on optical observations (Hedman et al., 2013), which predicted similar density to the Janus/Epimetheus ring. Figure S2 compares a radial brightness profile from the optical observations (Horányi et al., 2009) and the RPWS measurements of micron-sized dust surface density (integrated vertically) in the Janus/Epimetheus ring (Ye et al., 2018) and around 64,000 km, where orbits 276–282 ring plane crossings took place (this study). RPWS measurements at these two places showed larger contrast than the optical data did. The relative brightness between Janus/Epimetheus ring (~150,600 km) and the orbit 280 ring plane crossing location (~63,800 km) is about 2–3 to 1. However, the brightness of radial distance 62,000–64,000 km is around the background noise level, so the real brightness might be much lower, which would be more consistent with RPWS observations.

The lack of micron-sized dust in this region is still not fully understood. Inside the main rings of Saturn, the Keplerian velocity becomes faster than the corotation speed of the background plasma, which puts a drag on the dust particles through either kinetic or Coulomb impacts. After losing speed, these particles cannot sustain their orbit and will fall into the atmosphere of Saturn.

A similar mechanism has been proposed to explain the precipitation of small dust particles (8,000 to 50,000 amu) from the main rings observed by Magnetospheric Imaging Instrument (MIMI) Ion and Neutral Camera (INCA) and Charge Energy Mass Spectrometer (CHEMS) instruments (Mitchell et al., 2018).

RPWS monopole measurements during the Grand Finale orbits revealed mostly positive hits, indicating a positive spacecraft potential. However, a spacecraft immersed in cold dense plasma, like in the ionosphere, would normally be charged negatively. Another interpretation of the positive hits would be related to the strong magnetic field close to Saturn, where the Larmor radius of the electrons from the impact plasma cloud are smaller than the dimension of the spacecraft. So the electrons in the impact plasma cloud will be reabsorbed by the spacecraft while the ions can escape due to their larger Larmor radius. After an impact on the spacecraft body, the spacecraft will be charged negatively, while the antenna potential remains unchanged. This will result in a positive potential difference between the E_w antenna and the spacecraft body, as would be observed by the WBR. However, the ion escape model would make the rise time of the impact signals longer, as the ions in the impact plasma cloud travels slower than the electrons. The increase in rise time was observed in the laboratory simulation when the bias potential of the model spacecraft body was switched from negative to positive (Ye, Kurth, Hospodarsky, Averkamp, Gurnett, Sternovsky, et al., 2016). Such an increase in rise time could be difficult to detect in our data due to the limited time resolution of the WBR data (36 μ s for the 10-kHz mode; the monopole antenna cannot be used with the 80-kHz mode).

5. Summary

On 26 April 2017, Cassini dove into the gap between Saturn's main ring and its atmosphere starting the 22 Grand Finale orbits. Contrary to our expectations, RPWS observed few micron dust impacts during the first 5 and last 10 proximal orbits, not enough for characterizing the size distribution. During the higher-altitude D ring crossings (orbits 276–282), RPWS detected more dust impacts with the density estimated to be about 2 orders of magnitude lower than that measured during the Ring Grazing orbits. The monopole antenna measurements of dust impacts near the D ring indicated that the spacecraft was charged positively (the impact signals were mostly positive, whereas at larger radial distances the impacts detected by the monopole antenna were mostly negative). The positive potential might be due to secondary electron emissions induced by kinetic ion/fast neutral impacts when the spacecraft cut through the deep ionosphere. It is also possible that the positive polarity is due to the strong magnetic field near Saturn, which allowed only the ions to

escape after impacts. The increase of the heavy negative ion concentration in Saturn's ionosphere could also be responsible for the positive spacecraft potential (Kim & Merlino, 2006). The decay time of the dust impact waveforms seems to be dependent on ionosphere plasma density, which showed variations up to 2 orders of magnitude from orbit to orbit.

Acknowledgments

This research was supported by NASA through contract 1415150 with the Jet Propulsion Laboratory and Deutsches Zentrum für Luft- und Raumfahrt (OH 1401). The data used in this study are available through the Planetary Data System (PDS) or from the authors. We thank Chris Piker and Darrelle Wilkinson for the timely postpass queries and fast access to the PDS format data and Joe Groene and Terry Averkamp for their valuable help with Cassini ephemeris and attitude information. The first author thanks Matthew Hedman for helpful discussions and providing the ISS ring profile data.

References

- Aubier, M. G., Meyer-Vernet, N., & Pedersen, B. M. (1983). Shot noise from grain and particle impacts in Saturn's ring plane. *Geophysical Research Letters*, *10*(1), 5–8. <https://doi.org/10.1029/GL010i001p00005>
- Burns, J. A., Hamilton, D. P., & Showalter, M. R. (2001). Dusty rings and circumplanetary dust: Observations and simple physics. In *Interplanetary Dust* (pp. 641–725). Berlin, Heidelberg: Springer.
- Collette, A., Grün, E., Malaspina, D., & Sternovsky, Z. (2014). Micrometeoroid impact charge yield for common spacecraft materials. *Journal of Geophysical Research: Space Physics*, *119*, 6019–6026. <https://doi.org/10.1002/2014JA020042>
- Cuzzi, J., Clark, R., Filacchione, G., French, R., Johnson, R., Marouf, E., & Spilker, L. (2009). Ring particle composition and size distribution. In *Saturn from Cassini-Huygens* (pp. 459–509). Dordrecht, Netherlands: Springer.
- de Pater, I., Martin, S. C., & Showalter, M. R. (2004). Keck near-infrared observations of Saturn's E and G rings during Earth's ring plane crossing in August 1995. *Icarus*, *172*(2), 446–454. <https://doi.org/10.1016/j.icarus.2004.07.012>
- Dong, Y., Hill, T. W., & Ye, S.-Y. (2015). Characteristics of ice grains in the Enceladus plume from Cassini observations. *Journal of Geophysical Research: Atmospheres*, *120*, 915–937. <https://doi.org/10.1002/2014JA020288>
- Grün, E. (1984). Impact ionization from gold, aluminum and PCB-Z. *ESA Special Publications*, *224*, 39–41.
- Gurnett, D. A., Grün, E., Gallagher, D., Kurth, W. S., & Scarf, F. L. (1983). Micron-sized particles detected near Saturn by the Voyager plasma wave instrument. *Icarus*, *53*(2), 236–254. [https://doi.org/10.1016/0019-1035\(83\)90145-8](https://doi.org/10.1016/0019-1035(83)90145-8)
- Gurnett, D. A., Kurth, W. S., Kirchner, D. L., Hospodarsky, G. B., Averkamp, T. F., Zarka, P., et al. (2004). The Cassini Radio and Plasma Wave Science investigation. *Space Science Reviews*, *114*(1–4), 395–463. <https://doi.org/10.1007/s11214-004-1434-0>
- Hedman, M. M., Burns, J. A., Hamilton, D. P., & Showalter, M. R. (2012). The three-dimensional structure of Saturn's E ring. *Icarus*, *217*(1), 322–338. <https://doi.org/10.1016/j.icarus.2011.11.006>
- Hedman, M. M., Burns, J. A., Nicolson, P. D., Cuzzi, J. N. (2013). Status report for dust hazards during F ring/proximal orbits, Cassini Project Science Group Meetings #45, Pasadena, CA, USA.
- Hedman, M. M., Burns, J. A., Tiscareno, M. S., Porco, C. C., Jones, G. H., Roussos, E., et al. (2007). The source of Saturn's G ring. *Science*, *317*(5838), 653–656. <https://doi.org/10.1126/science.1143964>
- Hedman, M. M., & Showalter, M. R. (2016). A new pattern in Saturn's D ring created in late 2011. *Icarus*, *279*, 155–165. <https://doi.org/10.1016/j.icarus.2015.09.017>
- Hedman, M. M., & Stark, C. C. (2015). Saturn's g and d rings provide nearly complete measured scattering phase functions of nearby debris disks. *The Astrophysical Journal*, *811*(1), p. 67.
- Hill, T. W., Thomsen, M. F., Tokar, R. L., Coates, A. J., Lewis, G. R., Young, D. T., et al. (2012). Charged nanograins in the Enceladus plume. *Journal of Geophysical Research*, *117*, A05209. <https://doi.org/10.1029/2011JA017218>
- Horányi, M. (1996). Charged dust dynamics in the solar system. *Annual Review of Astronomy and Astrophysics*, *34*(1), 383–418. <https://doi.org/10.1146/annurev.astro.34.1.383>
- Horányi, M., Burns, J. A., Hedman, M. M., Jones, G. H., & Kempf, S. (2009). Diffuse rings. In *Saturn from Cassini-Huygens* (pp. 511–536). Netherlands: Springer.
- Horányi, M., Juhasz, A., & Morfill, G. E. (2008). Large-scale structure of Saturn's E ring. *Geophysical Research Letters*, *35*, L04203. <https://doi.org/10.1029/2007gl032726>
- Hsu, H. W., Schmidt, J., Kempf, S., Postberg, F., Moragas-Klostermeyer, G., Seiß, M., et al. (2018). In situ collection of dust grains falling from Saturn's rings into its atmosphere. *Science*. <https://doi.org/10.1126/science.aat3185>
- Jones, G. H., Arridge, C. S., Coates, A. J., Lewis, G. R., Kanani, S., Wellbrock, A., et al. (2009). Fine jet structure of electrically charged grains in Enceladus' plume. *Geophysical Research Letters*, *36*, L16204. <https://doi.org/10.1029/2009GL038284>
- Kim, S. H., & Merlino, R. L. (2006). Charging of dust grains in a plasma with negative ions. *Physics of Plasmas*, *13*(5), 052118.
- Krupp, N., Roussos, E., Paranicas, C., Mitchell, D. G., Kollmann, P., Ye, S., et al. (2017). Energetic electron measurements near Enceladus by Cassini during 2005–2015. *Icarus*, *306*, 256–274. <https://doi.org/10.1016/j.icarus.2017.10.022>
- Kurth, W. S., Averkamp, T. F., Gurnett, D. A., & Wang, Z. (2006). Cassini RPWS observations of dust in Saturn's E ring. *Planetary and Space Science*, *54*(9–10), 988–998. <https://doi.org/10.1016/j.pss.2006.05.011>
- Meyer-Vernet, N., Lecacheux, A., Kaiser, M. L., & Gurnett, D. A. (2009). Detecting nanoparticles at the radio frequencies: Jovian dust stream impacts on Cassini/RPWS. *Geophysical Research Letters*, *36*, L03103. <https://doi.org/10.1029/2008GL036752>
- Meyer-Vernet, N., Lecacheux, A., & Pedersen, B. M. (1996). Constraints on Saturn's E ring from the Voyager 1 radio astronomy instrument. *Icarus*, *123*(1), 113–128. <https://doi.org/10.1006/icar.1996.0145>
- Meyer-Vernet, N., Moncuquet, M., Issautier, K., & Schippers, P. (2017). Frequency range of dust detection in space with radio and plasma wave receivers: Theory and application to interplanetary nanodust impacts on Cassini. *Journal of Geophysical Research: Space Physics*, *122*, 8–22. <https://doi.org/10.1002/2016JA023081>
- Mitchell, D. G., Perry, M. E., Hamilton, D. C., Westlake, J. H., Kollmann, P., Smith, H. T., et al. (2018). Dust grains fall from Saturn's D-ring into its equatorial upper atmosphere. *Science*. <https://doi.org/10.1126/science.aat2236>
- Morooka, M. W., Wahlund, J.-E., Andrews, D., Persoon, A. M., Ye, S.-Y., Kurth, W. S., et al. (2018). The dusty plasma disk around the Janus/Epimetheus ring. *Journal of Geophysical Research: Space Physics*, *123*, 4668–4678. <https://doi.org/10.1002/2017JA024917>
- Nicholson, P. D., Showalter, M. R., & Dones, L. (1996). Observations of Saturn's ring-plane crossing in August and November. *Science*, *272*(5261), 509–515. <https://doi.org/10.1126/science.272.5261.509>
- Nouzak, L., Hsu, S., Malaspina, D., Thayer, F. M., Ye, S.-Y., Pavlu, J., et al. (2017). Laboratory modeling of dust impact detection by the Cassini spacecraft. *Planetary and Space Science*, *156*, 85–91. <https://doi.org/10.1016/j.pss.2017.11.014>
- Nouzak, L., Pavlu, J., Nemecek, Z., Safrankova, J., Khalili, A., Hsu, S., et al. (2017). *Laboratory investigation of dust impacts on antennas of the Cassini model spacecraft*. Vienna, Austria: EGU.
- O'Shea, E., Sternovsky, Z., & Malaspina, D. M. (2017). Interpreting dust impact signals detected by the STEREO spacecraft. *Journal of Geophysical Research: Space Physics*, *122*, 11,864–11,873. <https://doi.org/10.1002/2017JA024786>

- Persoon, A. M., Kurth, W. S., Gurnett, D. A., Groene, J. B., Sulaiman, A. H., & Wahlund, J. E. (2018). Electron density distributions in Saturn's ionosphere. *Geophysical Research Letters*, *45*.
- Schippers, P., Meyer-Vernet, N., Lecacheux, A., Belheouane, S., Moncuquet, M., Kurth, W. S., et al. (2015). Nanodust detection between 1 and 5 AU using Cassini wave measurements. *The Astrophysical Journal*, *806*(1), 77. <https://doi.org/10.1088/0004-637X/806/1/77>
- Schippers, P., Meyer-Vernet, N., Lecacheux, A., Kurth, W. S., Mitchell, D. G., & André, N. (2014). Nanodust detection near 1 AU from spectral analysis of Cassini/Radio and Plasma Wave Science data. *Geophysical Research Letters*, *41*, 5382–5388. <https://doi.org/10.1002/2014GL060566>
- Showalter, M. R., Cuzzi, J. N., & Larson, S. M. (1991). Structure and particle properties of Saturn's E ring. *Icarus*, *94*(2), 451–473. [https://doi.org/10.1016/0019-1035\(91\)90241-K](https://doi.org/10.1016/0019-1035(91)90241-K)
- Showalter, M. R. (1996). Saturn's D ring in the Voyager images. *Icarus*, *124*(2), 677–689. <https://doi.org/10.1006/icar.1996.0241>
- Spahn, F., Albers, N., Hörning, M., Kempf, S., Krivov, A. V., Makuch, M., & Sremčević, M. (2006). E ring dust sources: Implications from Cassini's dust measurements. *Planetary and Space Science*, *54*(9–10), 1024–1032. <https://doi.org/10.1016/j.pss.2006.05.022>
- Spahn, F., Schmidt, J., Albers, N., Hörning, M., Makuch, M., Seif, M., et al. (2006). Cassini dust measurements at Enceladus and implications for the origin of the E ring. *Science*, *311*(5766), 1416–1418. <https://doi.org/10.1126/science.1121375>
- Srama, R., Ahrens, T. J., Altobelli, N., Auer, S., Bradley, J. G., Burton, M., et al. (2004). The Cassini Cosmic Dust Analyzer. *Space Science Reviews*, *114*(1–4), 465–518. <https://doi.org/10.1007/s11214-004-1435-z>
- Sulaiman, A. H., Kurth, W. S., Persoon, A. M., Menietti, J. D., Farrell, W. M., Ye, S. Y., et al. (2017). Intense harmonic emissions observed in Saturn's ionosphere. *Geophysical Research Letters*, *44*, 12,049–12,056. <https://doi.org/10.1002/2017GL076184>
- Wahlund, J.-E., Morooka, M. W., Hadid, L. Z., Persoon, A. M., Farrell, W. M., Gurnett, D. A., et al. (2018). In situ measurements of Saturn's ionosphere show that it is dynamic and interacts with the rings. *Science*, eaao4134. <https://doi.org/10.1126/science.aao4134>
- Wang, Z., Gurnett, D. A., Averkamp, T. F., Persoon, A. M., & Kurth, W. S. (2006). Characteristics of dust particles detected near Saturn's ring plane. *Planetary and Space Science*, *54*(9–10), 957–966. <https://doi.org/10.1016/j.pss.2006.05.015>
- Williams, G. A., & Murray, C. D. (2011). Stability of co-orbital ring material with applications to the Janus–Epimetheus system. *Icarus*, *212*(1), 275–293. <https://doi.org/10.1016/j.icarus.2010.11.038>
- Ye, S.-Y., Gurnett, D. A., & Kurth, W. S. (2016). In-situ measurements of Saturn's dusty rings based on dust impact signals detected by Cassini RPWS. *Icarus*, *279*, 51–61. <https://doi.org/10.1016/j.icarus.2016.05.006>
- Ye, S.-Y., Gurnett, D. A., Kurth, W. S., Averkamp, T. F., Kempf, S., Hsu, H. W., et al. (2014). Properties of dust particles near Saturn inferred from voltage pulses induced by dust impacts on Cassini spacecraft. *Journal of Geophysical Research: Space Physics*, *119*, 6294–6312. <https://doi.org/10.1002/2014ja020024>
- Ye, S.-Y., Kurth, W. S., Hospodarsky, G. B., Averkamp, T. F., & Gurnett, D. A. (2016). Dust detection in space using the monopole and dipole electric field antennas. *Journal of Geophysical Research: Space Physics*, *121*, 11,964–11,972. <https://doi.org/10.1002/2016JA023266>
- Ye, S.-Y., Kurth, W. S., Hospodarsky, G. B., Averkamp, T. F., Gurnett, D. A., Sternovsky, Z., et al. (2016). *Dust impact signals detected by Cassini RPWS: Observations and laboratory experiments*. San Francisco: American Geophysical Union, Fall Meeting.
- Ye, S.-Y., Kurth, W. S., Hospodarsky, G. B., Persoon, A. M., Gurnett, D. A., Morooka, M., et al. (2018). Cassini RPWS dust observation near Janus and Epimetheus orbits. *Journal of Geophysical Research: Space Physics*, *123*, 4952–4960. <https://doi.org/10.1029/2017JA025112>
- Zaslavsky, A. (2015). Floating potential perturbations due to micrometeoroid impacts: Theory and application to S/WAVES data. *Journal of Geophysical Research: Space Physics*, *120*, 855–867. <https://doi.org/10.1002/2014JA020635>